



Contents lists available at ScienceDirect

Journal of Magnetic Resonance

journal homepage: www.elsevier.com/locate/jmr

Communication

Fast acquisition of high resolution 4-D amide–amide NOESY with diagonal suppression, sparse sampling and FFT-CLEAN

Jon W. Werner-Allen, Brian E. Coggins, Pei Zhou *

Department of Biochemistry, Duke University Medical Center, Durham, NC 27710, United States

ARTICLE INFO

Article history:

Received 4 December 2009

Revised 18 February 2010

Available online 21 February 2010

Keywords:

Diagonal suppression

TROSY-NOESY-TROSY

TNT

Fast NMR

Sparse sampling

FFT-CLEAN

ABSTRACT

Amide–amide NOESY provides important distance constraints for calculating global folds of large proteins, especially integral membrane proteins with β -barrel folds. Here, we describe a diagonal-suppressed 4-D NH–NH TROSY-NOESY-TROSY (ds-TNT) experiment for NMR studies of large proteins. The ds-TNT experiment employs a spin state selective transfer scheme that suppresses diagonal signals while providing TROSY optimization in all four dimensions. Active suppression of the strong diagonal peaks greatly reduces the dynamic range of observable signals, making this experiment particularly suitable for use with sparse sampling techniques. To demonstrate the utility of this method, we collected a high resolution 4-D ds-TNT spectrum of a 23 kDa protein using randomized concentric shell sampling (RCSS), and we used FFT-CLEAN processing for further reduction of aliasing artifacts – the first application of these techniques to a NOESY experiment. A comparison of peak parameters in the high resolution 4-D dataset with those from a conventionally-sampled 3-D control spectrum shows an accurate reproduction of NOE crosspeaks in addition to a significant reduction in resonance overlap, which largely eliminates assignment ambiguity. Likewise, a comparison of 4-D peak intensities and volumes before and after application of the CLEAN procedure demonstrates that the reduction of aliasing artifacts by CLEAN does not systematically distort NMR signals.

© 2010 Elsevier Inc. All rights reserved.

1. Introduction

Amide–amide NOESY provides valuable distance constraints for calculating global folds of large proteins, which are especially important for proteins with high β -sheet content. In extreme cases, such as β -barrel proteins, amide–amide constraints alone can be sufficient to define the overall topology. Amide–amide NOESY is also useful for defining secondary structure elements and for confirming and extending backbone amide assignments. Protein deuteration [1,2] and the development of TROSY [3,4] have greatly improved the sensitivity of the amide–amide NOESY experiment by minimizing signal loss from transverse relaxation, a major obstacle for NMR studies of large proteins.

The spectral complexity of NOESY experiments with large proteins presents another serious challenge for structural studies. In 3-D NOESY experiments, the large number of proton signals can create severe resonance overlap, frustrating assignment efforts and reducing distance constraint accuracy. While this problem can be largely eliminated by recording high resolution 4-D NOESY spectra, the measurement times required for conventional Nyquist

sampling of individual dimensions have restricted the acquisition of 4-D NOESY data to very low resolution. However, the increased sensitivity of NMR experiments benefiting from improved probe technology, protein deuteration, and TROSY methods has made it possible to apply sparse sampling methods for more efficient collection of high resolution 4-D spectra with reduced peak overlap and assignment ambiguity. Indeed, significant efforts have been devoted to the development and optimization of sparse sampling patterns in the time domain as well as methods for reconstructing spectral information from sparsely sampled datasets [5–32]. Recently, we described a sparse sampling scheme – randomized concentric shell sampling (RCSS) – for collecting high resolution 4-D NMR spectra [33], which gives greater sensitivity and fewer artifacts than the radial sampling method. Using RCSS data collection, we recorded a high resolution 4-D HCCH-TOCSY spectrum for protein G's B1 domain in ~21 h, or 1.2% of the time required for conventional sampling of the same experiment at equivalent resolution.

The inherent drawback of using sparse sampling schemes is the appearance of aliasing artifacts resulting from the violation of the Nyquist theorem [9,34]. Importantly, the level of aliasing artifacts for each signal is proportional to the signal amplitude. This is particularly problematic in NOESY spectra, where the dynamic range of signal amplitudes is very large, as aliasing artifacts from strong

* Corresponding author. Address: 273 Sands Bldg., Research Dr., Durham, NC 27710, USA. Fax: +1 (919) 684 8885.

E-mail address: peizhou@biochem.duke.edu (P. Zhou).

diagonal peaks may overshadow weak NOE crosspeaks – even with optimized arrangements of sampling points that reduce the reinforcement of these artifacts. A simple solution to this problem is to suppress the diagonal signals. Among the methods of diagonal suppression [35–38], the approach based on TROSY spin state selection is the most attractive for large proteins, as it has the added benefit of reducing transverse relaxation losses. Such an approach has been demonstrated in the 3-D NH–NH NOESY experiment [39–41], but these implementations cannot be extended directly to 4-D experiments, as they lack a polarization transfer element that permits nitrogen chemical shift evolution after the NOE mixing period.

In this paper, we describe a diagonal-suppressed TROSY-NOESY-TROSY (ds-TNT) pulse sequence with a novel single transition-to-single transition polarization transfer element that allows transverse relaxation optimized chemical shift evolution in all four dimensions. We apply RCSS data collection and FFT-CLEAN processing to record a high resolution 4-D ds-TNT spectrum of a 23 kDa protein with low artifact levels and well-suppressed diagonal peaks. Representative examples demonstrate the reduced signal overlap and assignment ambiguity in this high resolution 4-D dataset. Finally, by comparison with peaks in a conventionally-sampled 3-D control spectrum, we show that sparse sampling and artifact reduction with CLEAN retain the linearity of NOE crosspeak information over the entire dynamic range recorded with the ds-TNT experiment.

2. Methods

2.1. 4-D NH–NH ds-TNT pulse sequence

The pulse sequence for the 4-D ds-TNT experiment (Fig. 1) can be separated into four main sections: the first TROSY selection with frequency labeling in t_1 (N_1) and t_2 (H_1), the NOE mixing period, a ‘reverse’ single transition-to-single transition polarization transfer (reverse ST2-PT), and the second TROSY selection with frequency labeling in t_3 (N_2) followed by detection in t_4 (H_2). The experiment begins with a sensitivity enhanced gradient selection of TROSY magnetization with suppression of the anti-TROSY coherence pathway [42]. Inversion of phases ϕ_2 and ϕ_{rec} and gradient G_2 controls coherence pathway selection while incrementing phase ϕ_3 (and phase ϕ_4 for water suppression) controls cosine–sine selection for the first two dimensions. Ignoring the t_3 (N_2) and t_4 (H_2) dimensions, recording the sensitivity enhanced signals in the first two dimensions yields the following pattern of frequency labeling:

$$\begin{aligned} S_{11} &= \cos(\omega_{N_1}t_1 + \omega_{H_1}t_2) \\ S_{12} &= \sin(\omega_{N_1}t_1 + \omega_{H_1}t_2) \\ S_{21} &= \cos(-\omega_{N_1}t_1 + \omega_{H_1}t_2) \\ S_{22} &= \sin(-\omega_{N_1}t_1 + \omega_{H_1}t_2) \end{aligned} \quad (1)$$

which can be resolved into quadrature components by standard procedures [41].

After the first spin state selective transfer, the TROSY coherence of spin 1 (which is N_α polarized) enters the NOE mixing period and is transferred to magnetization in spin 2, creating both N_α and N_β polarization:

$$\begin{aligned} N_\alpha^1 H_z^1 \xrightarrow{\text{NOE mixing}} N_\alpha^1 H_z^1 (\text{diagonal}) + N_\alpha^1 H_z^2 (\text{crosspeak}) &= N_\alpha^1 H_z^1 (\text{diagonal}) \\ &+ N_\alpha^1 N_\beta^2 H_z^2 (\text{crosspeak}) + N_\beta^1 N_\beta^2 H_z^2 (\text{crosspeak}) \end{aligned} \quad (2)$$

The N_β polarization of the spin 2 coherence created during the mixing period ($N_\alpha^1 N_\beta^2 H_z^2$) provides the means for selectively suppressing the diagonal coherence, which is still in the N_α state. Before eliminating the diagonal signals, however, the nitrogen chemical shift of spin 2 must be recorded to permit four dimensional data collection. This requires a specially-designed reverse ST2-PT that simultaneously achieves four coherence transfers:

$$\begin{aligned} N_\alpha^1 H_z^1 &\rightarrow N_z^1 H_z^1 \\ N_\alpha^1 &\rightarrow H_z^1 \\ N_\alpha^2 H_z^2 &\rightarrow N_z^2 H_z^2 \\ N_\beta^2 H_z^2 &\rightarrow -N_z^2 H_z^2 \end{aligned} \quad (3)$$

This yields the following coherence terms immediately before the 90° ^{15}N pulse that starts t_3 :

$$\begin{aligned} \xrightarrow{\text{reverse ST2-PT}} N_z^1 H_z^1 (\text{diagonal}) + H_z^1 N_z^2 H_z^2 (\text{crosspeak}) \\ - H_z^1 N_z^2 H_z^2 (\text{crosspeak}) \end{aligned} \quad (4)$$

Thus, the desired magnetization – the N_β polarized coherence of spin 2 ($N_\alpha^1 N_\beta^2 H_z^2$) – is transferred to H_β polarized coherence ($H_z^1 N_z^2 H_z^2$) to set up TROSY collection in t_3 (N_2). This also converts the N_α^1 coherence term of spin 2 (transferred during NOE mixing) to H_α^1 coherence so that it does not interfere with frequency labeling. Additionally, the diagonal magnetization ($N_\alpha^1 H_z^1$) and the N_α polarized coherence of spin 2 ($N_\alpha^1 N_\alpha^2 H_z^2$) are converted to anti-TROSY coherence for t_3 .

Diagonal signals are suppressed by the second TROSY transfer element, which selects for the TROSY coherence pathway of spin 2 while suppressing the anti-TROSY pathways of spin 2 and spin

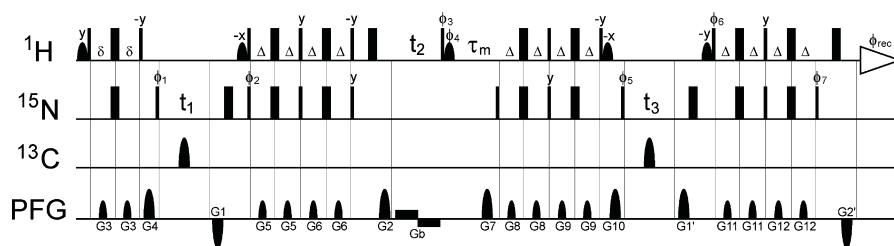


Fig. 1. Pulse sequence for the 4-D ds-TNT experiment. Narrow and wide bars represent 90° and 180° pulses, respectively. All pulses are applied along the x -axis unless noted otherwise. Ninety degree selective water pulses are indicated by shaped bars. The delays are $\delta = 2.4$ ms, $\Delta = 2.75$ ms, and $\tau_m = 200$ ms. Phase cycling is $\phi_1 = [2x, 2(-x)]$, $\phi_2 = [-x]$, $\phi_3 = [y]$, $\phi_4 = [-y]$, $\phi_5 = [x, -x]$, $\phi_6 = [x]$, $\phi_7 = [y]$, and $\phi_{\text{rec}} = [x, -x, -x, x]$. Inversion of ϕ_3 (and ϕ_4 for water suppression) at even numbered lattice points in t_2 introduces a frequency shift of $\text{sw}_2/2$ to the H_1 dimension in order to center the amide signals while leaving the transmitter frequency on water. This was found to provide better water suppression than the alternative: shifting the transmitter frequency before t_2 (H_1) and applying an off-resonance water flip-back pulse (for ϕ_4). Axial peaks are removed by setting $(\phi_1 + 180^\circ, \phi_{\text{rec}} + 180^\circ)$ and $(\phi_5 + 180^\circ, \phi_{\text{rec}} + 180^\circ)$ at even numbered lattice points in F1 and F3, respectively. Hypercomplex data collection for the two SE TROSY elements requires inversion of ϕ_2 , ϕ_{rec} , and G_2 for the F1 dimension and inversion of ϕ_6 , ϕ_7 and G_2' for the F3 dimension. Cosine–sine selection for the F1/F2 dimensions is controlled by incrementing phase ϕ_3 (and phase ϕ_4 for water suppression). Gradient durations and field strengths are $G_1 = (2$ ms, -18.38 G/cm), $G_2 = (0.2$ ms, 18.32 G/cm), $G_1' = (2$ ms, 20.42 G/cm), $G_2' = (0.2$ ms, -20.36 G/cm), $G_3 = (0.5$ ms, 11.64 G/cm), $G_4 = (1$ ms, -18.99 G/cm), $G_5 = (0.5$ ms, 17.77 G/cm), $G_6 = (0.5$ ms, 15.72 G/cm), $G_7 = (1$ ms, 23.89 G/cm), $G_8 = (0.5$ ms, 10.01 G/cm), $G_9 = (0.5$ ms, 10.82 G/cm), $G_{10} = (1$ ms, 21.03 G/cm), $G_{11} = (0.5$ ms, 10.41 G/cm), $G_{12} = (0.5$ ms, 14.09 G/cm). A small refocusing gradient is applied during t_2 (G_2) to suppress water radiation damping.

1. This transfer uses the ST2-PT method [43] to convert the desired crosspeak magnetization to $N_{\beta}^{\prime}N_{\alpha}^{\prime}H_{\pm}^{\prime}$ for direct detection, with coherence pathway selection controlled by inversion of phases ϕ_6 and ϕ_7 and gradient G_2' . While the ST2-PT scheme is more susceptible to signal loss during coherence transfer compared to the Nietispach technique used in the first TROSY transfer [42], the ST2-PT method proved to be more effective at suppressing signals from sidechain amino groups.

2.2. Randomized concentric shell sampling and the CLEAN algorithm

To collect a 4-D ds-TNT spectrum at high resolution, we employed cosine-weighted randomized concentric shell sampling (RCSS) – an extension of the 3-D concentric ring sampling (CRS) method [10], which was developed as an alternative to radial sampling with better sensitivity and fewer artifacts [33]. In the RCSS method, points are set on a series of evenly spaced shells, where the distribution of points on each shell is uniform. The distribution of points across shells can be adjusted based on the properties of the signal being collected. In order to prevent the reinforcement of artifacts generated by regular patterns of sampling points, each shell is rotated randomly about all three dimensions. Finally, the sampling pattern is adapted to a fine Cartesian grid to enable rapid processing by the fast Fourier transform (FFT) without causing a significant increase in artifact levels [33].

The CLEAN algorithm was used to reduce aliasing artifacts produced by RCSS data collection. Our implementation of CLEAN is an iterative process that (1) finds the strongest peak in a spectrum, (2) generates a replica, or component, of the peak, (3) calculates the artifact pattern of the component based on knowledge of the sampling scheme, and (4) subtracts the component and its sampling artifacts from the spectrum [33]. While CLEAN has been traditionally applied with fitted lineshapes for each component, the use of non-decaying components (which treats each peak as a set of discrete points) is equally effective and eliminates the need to estimate linewidths. The algorithm is terminated when the noise level has stabilized or when all peaks with significant intensity have been removed. Artifact-free components are then convolved with an abridged point response function derived from the sampling pattern and added back to yield a spectrum with reduced sampling artifacts.

2.3. 4-D ds-TNT with RCSS sampling and FFT-CLEAN processing

The ds-TNT pulse sequence was tested with a 1 mM sample of $^2\text{H}/^{13}\text{C}/^{15}\text{N}$ -labeled C13S Ssu72, a 23 kDa catalytically inactive phosphatase. Data was collected on a Varian INOVA 800 MHz spectrometer equipped with a triple-resonance cold probe with Z-axis gradients. For the 4-D ds-TNT experiment, the RCSS sampling pattern contained 3189 points distributed with cosine-weighting over 64 shells and digitized on a $64 \times 64 \times 64$ grid. Simple modification of the ds-TNT pulse sequence code allowed sampling from an explicit schedule of evolution times. The maximum evolution times were 0.0138 s for H_1 (4650 Hz spectral width) and 0.0237 s for N_1 and N_2 (2700 Hz spectral width). The total measurement time was 48 h. The contribution of each sampling point for the FFT processing was calculated as its cosine-weighted Voronoi volume. After FFT computation of the 4-D spectrum, the CLEAN algorithm was run to reduce sampling artifacts with a loop gain setting of 10%, a stopping threshold of 1%, and a 500 iteration maximum run for each cube as previously described [33]. The processing time for the entire 4-D dataset was ~ 40 min on a quad-core 2.4 GHz personal computer.

Three dimensional (N_1, N_2, H_2) and (H_1, N_2, H_2) control spectra were collected using conventional sampling, with spectral widths identical to those used in the 4-D experiment. The maximum evolution times for the 3-D (N_1, N_2, H_2) experiment were 0.0237 s (64 complex points) for N_1 and N_2 with a total measurement time of 32 h (4 scans per FID). For the 3-D (H_1, N_2, H_2) experiment, the maximum evolution times were 0.0103 s (48 complex points) for H_1 and 0.0237 s (64 complex points) for N_2 with a total measurement time of 48 h. The resolution of the H_1 dimension was extended to 0.0138 s (64 complex points) with linear prediction. Both experiments were processed with a cosine window function and zero-filled to 128 points in each indirect dimension.

The effect of RCSS sampling and CLEAN processing on the analysis of the NH–NH NOESY data was assessed with peak intensities and volumes using a set of 564 non-overlapping peaks assigned in the 4-D ds-TNT spectrum. For comparisons between 3-D and 4-D spectra, peak intensity was found to be a more reliable measure than peak volume due to increased signal overlap in the 3-D spectrum. A set of 376 crosspeaks from the (H_1, N_2, H_2) 3-D ds-TNT spectrum was used for comparisons with the 4-D dataset. About 12% of the 3-D peaks correspond to two or more 4-D peaks that

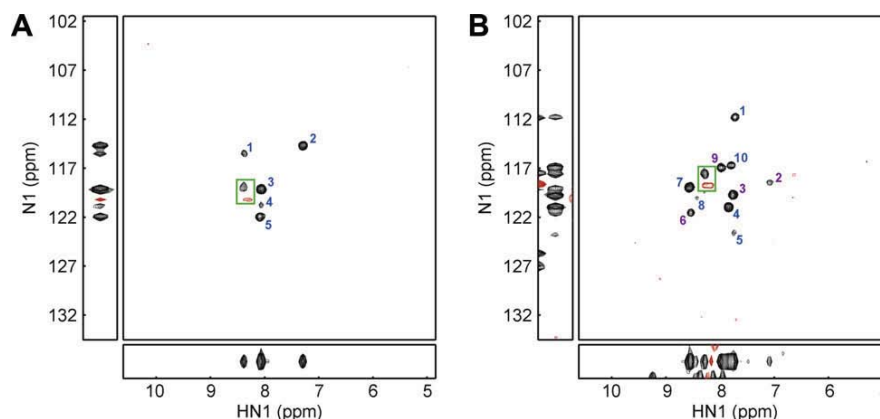


Fig. 2. Representative planes from the 4-D ds-TNT dataset. Corresponding strips are from 3-D ds-TNT control spectra collected with conventional sampling. Residual diagonal signals are boxed in green with negative contours in red. Panel (A) shows crosspeaks from residue I176 of C13S Ssu72 to D173 (1), N174 (2), D175 (3), D177 (5) and E178 (4). Panel (B) contains crosspeaks from two overlapped residues, L72 and N92. Blue numbers denote crosspeaks from L72 to Y69 (8), R70 (10), D71 (4), E73 (7), S74 (1) and K75 (5) and purple numbers correspond to crosspeaks from N92 to D90 (6), R91 (3), R93 (9) and R94 (2).

overlapped in the 3-D spectrum, and in these cases, a summation of the 4-D peak intensities was used.

3. Results

3.1. 4-D NH–NH TROSY-NOESY-TROSY with diagonal suppression

We tested our ds-TNT experiment by collecting a 4-D spectrum of the 23 kDa C13S Ssu72 protein with RCSS sampling and FFT-CLEAN processing. Fig. 2 shows two representative examples of F1/F2 planes taken at the F3/F4 positions of residue I176 and the overlapped residues L72/N92. The strips are from the corresponding positions in the conventionally collected 3-D control spectra. Residual diagonal signals are boxed in green. The pattern of residual diagonal peaks is generated by two processes: (1) incomplete suppression of the anti-TROSY coherence pathway by the spin state selective transfer elements and (2) ^{15}N spin state relaxation during the NOE mixing period. In all cases, the diagonals are well-suppressed, with residual intensities matching medium-sized NOESY crosspeaks.

3.2. Application of RCSS data collection and FFT-CLEAN to NOESY

While RCSS data collection and FFT-CLEAN processing have been applied successfully to a 4-D HCCH-TOCSY experiment [33], NOESY presents a new challenge as the preservation of the inherent distance constraint information requires a linear reproduction of peak shapes and intensities over a large dynamic range. To gauge the affects of RCSS data collection on the 4-D ds-TNT NOESY experiment, we compared the intensities of 376 crosspeaks in the 3-D ($H1, N2, H2$) ds-TNT control with their counterparts in the FFT-processed 4-D spectrum. The results are plotted in Fig. 3. The comparison of 3-D and 4-D peak intensities shows a very strong and consistent linear relationship that can be fit to a linear regression (y -intercept set at zero) with an R^2 value of 0.9655. This result is consistent with the observation by Kazimierczuk and co-workers [19] that the FFT is a linear process and does not distort the crosspeak information in a systematic fashion.

We next evaluated the effect of the CLEAN procedure on the 4-D dataset. Noise levels for all 128 ($N1, H1, N2$) cubes in the 4-D spectrum were measured with and without artifact removal. This analysis showed a range of noise reductions with maximum benefits for cubes with strong signals. The largest decrease in apparent noise was 22%. We then tested the CLEAN procedure for retention of NOESY distance information with a set of 564 crosspeaks from the 4-D ds-TNT spectrum. The intensity and volume of each peak were calculated before and after the application of CLEAN, and the results are plotted in Fig. 4. The excellent linear fits to this data demonstrate that CLEAN does not systematically distort signal information for the ds-TNT experiment.

4. Discussion

4.1. ds-TNT for sparse sampling

Amide–amide NOESY is one of the central experiments used to calculate global folds for large proteins and to verify and extend the assignment of backbone amide groups. However, the analysis of amide–amide NOESY data from high molecular weight proteins is hindered by the large number of signals that leads to resonance overlap and assignment ambiguity. Increasing the dimensionality of these datasets while maintaining high digital resolution is the most straightforward solution to both problems. The diagonal-suppressed NH–NH TROSY-NOESY-TROSY (ds-TNT) experiment presented here is designed for structural studies of large protein

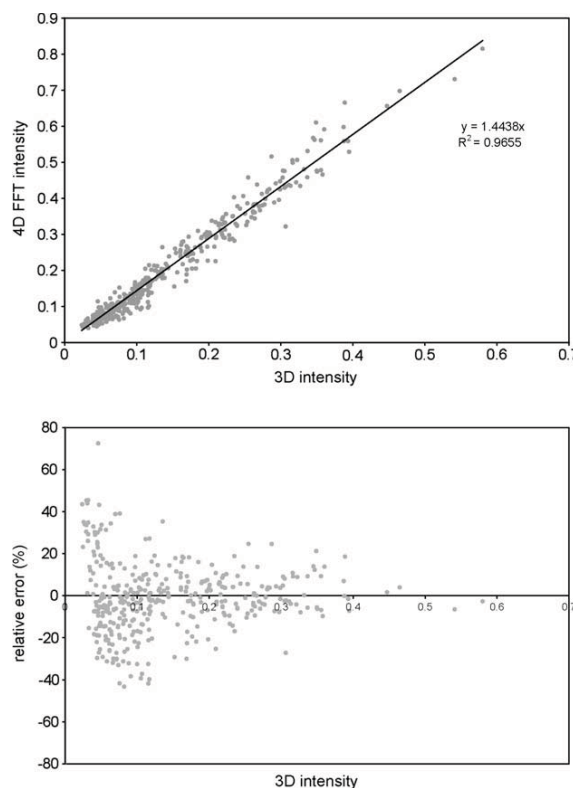


Fig. 3. Comparison of peak intensities for 3-D and 4-D ds-TNT data. Peak intensities from 376 NOESY crosspeaks were calculated from the conventionally-sampled 3-D ($H1, N2, H2$) ds-TNT dataset and the RCSS 4-D ds-TNT dataset with FFT processing. The data were fit to a linear model ($y = kx$) with an R^2 value of 0.9655. Relative percentage errors with respect to the 3-D peak intensities are plotted in the lower panel.

targets; accordingly, it has two features that should make it exceptionally beneficial to these studies.

The first key feature of the ds-TNT experiment is TROSY spin state selection in all four dimensions. As the molecular weight of NMR targets increases, TROSY optimization becomes more important, both for minimizing relaxation losses and for reducing peak overlap by sharpening linewidths. Suppression of diagonal signals is the second advantage of the ds-TNT experiment. Importantly, this suppression is achieved by manipulating the spin state selective transfers which are *already used* for TROSY selection, eliminating the loss in sensitivity or increase in spectrometer time inherent to other methods [36,37]. As shown in Fig. 2, the ds-TNT experiment reduces the strength of diagonal signals to that of medium-sized NOESY crosspeaks. This diagonal suppression allows the identification of crosspeaks that lie near diagonal peaks, increasing the completeness of NOESY assignment and potentially improving the accuracy of structure calculations; however, the most compelling reason for diagonal suppression comes from the application of sparse sampling schemes: the reduction of sampling artifacts. As the artifacts generated by each peak are proportional to its intensity, strong diagonal peaks produce strong artifact patterns that can obscure weak NOESY crosspeaks. Therefore, diagonal suppression makes the ds-TNT experiment particularly attractive for high dimensionality data collection with many of the sparse sampling methods.

4.2. Application of sparse sampling and FFT-CLEAN to NOESY

While RCSS data collection and CLEAN processing have been applied successfully to 4-D HCCH-TOCSY [33], NOESY experiments

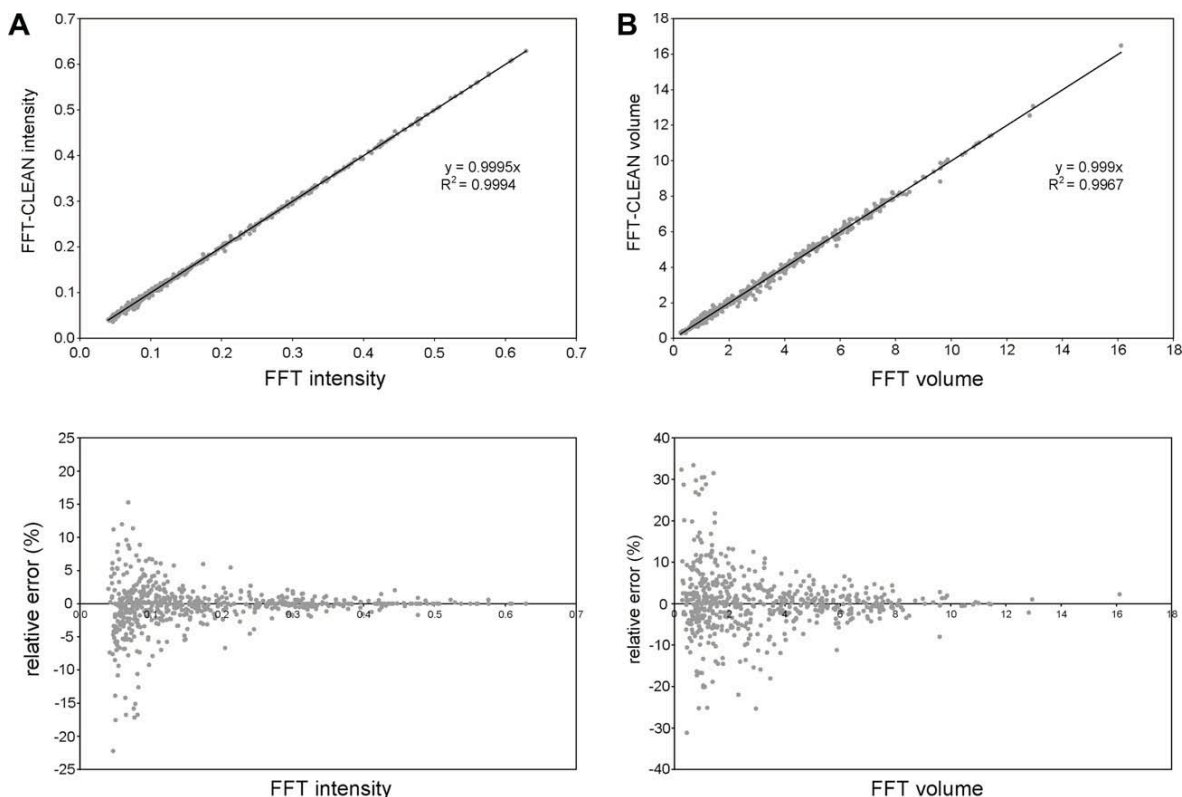


Fig. 4. Comparison of 4-D ds-TNT peaks with FFT and FFT-CLEAN processing. NOESY crosspeaks from the RCSS 4-D ds-TNT dataset were used to assess the effect of artifact reduction with the CLEAN algorithm on peak intensities and volumes. In panel (A), peak intensities are plotted with and without CLEAN processing, giving a linear fit of $y = 0.9995x$ with an R^2 value of 0.9994. In panel (B), peak volumes are plotted with and without CLEAN processing, giving a linear fit of $y = 0.999x$ with an R^2 value of 0.9967. For panels (A) and (B), relative percentage errors between FFT and FFT-CLEAN processing are plotted in the lower graphs.

present unique challenges to these methods, as the distance constraint information inherent in peak volumes must be faithfully reproduced to avoid bias in structure calculations. The comparison of crosspeak intensities for the 4-D ds-TNT spectrum and 3-D control (Fig. 3) shows that essential peak information is replicated with consistent accuracy in the sparsely sampled dataset. Furthermore, the strong linear relationship between 4-D peak intensities and volumes before and after CLEAN processing (Fig. 4) demonstrates that the removal of aliasing artifacts does not systematically alter distance constraint information. Taken together, we conclude that RCSS data collection and FFT-CLEAN processing can be applied to the 4-D ds-TNT experiments without sacrificing the accuracy of subsequent structure calculations. The advantages of high resolution 4-D NOESY data can be clearly appreciated in the example planes of Fig. 2 where signal overlap in the control 3-D ds-TNT spectrum would preclude the complete and accurate assignment of crosspeaks.

The feasibility of applying sparse sampling techniques to collect high resolution 4-D ds-TNT spectra is particularly exciting in light of the time savings over conventional sampling methods. A 4-D ds-TNT spectrum recorded conventionally with 64 point resolution in each indirect dimension (after two fold linear prediction) would require nearly 3 weeks; the 4-D ds-TNT spectrum presented here was recorded with 64 point resolution in only 48 h, a more than 10-fold reduction in spectrometer time. The success in applying RCSS data collection and FFT-CLEAN processing to obtain high resolution 4-D NH–NH NOESY should help extend NMR structure determination to high molecular weight targets.

5. Conclusions

We have introduced a 4-D diagonal-suppressed TROSY-NOESY-TROSY (4-D ds-TNT) experiment for collecting amide–amide distance constraints, which is specifically designed for use with large proteins and particularly well-suited for the application of sparse sampling methods. The key element of this pulse sequence is a spin state selective transfer element that permits frequency labeling with TROSY optimization in all four dimensions. Using the ds-TNT experiment, we also present the first application of RCSS data collection and FFT-CLEAN processing to high resolution 4-D NOESY of a 23 kDa protein. Analysis of 376 peaks in the 4-D dataset and a 3-D control spectrum collected with conventional sampling demonstrates that peak intensities are reproduced accurately in the sparsely sampled data. Likewise, a comparison of intensities and volumes for 564 peaks in the 4-D spectrum before and after application of the CLEAN procedure shows that peak volumes are unaffected by the removal of aliasing artifacts. By running the ds-TNT experiment with RCSS data collection and FFT-CLEAN processing, we are able to collect a high resolution 4-D dataset with low artifact levels in only 2 days, making this experiment a valuable tool for structural studies of large proteins by NMR.

Acknowledgments

This work was supported by the National Institutes of Health (GM079376), the Whitehead Foundation and the Duke University Bridge Fund.

References

- [1] D.M. LeMaster, F.M. Richards, NMR sequential assignment of *Escherichia coli* thioredoxin utilizing random fractional deuteration, *Biochemistry* 27 (1988) 142–150.
- [2] B.T. Farmer 2nd, R.A. Venters, NMR of perdeuterated large proteins, *Biol. Magn. Reson.* 16 (1999) 75–120.
- [3] K. Pervushin, R. Riek, G. Wider, K. Wüthrich, Attenuated T₂ relaxation by mutual cancellation of dipole–dipole coupling and chemical shift anisotropy indicates an avenue to NMR structures of very large biological macromolecules in solution, *Proc. Natl. Acad. Sci. USA* 94 (1997) 12366–12371.
- [4] K. Pervushin, Impact of transverse relaxation optimized spectroscopy (TROSY) on NMR as a technique in structural biology, *Q. Rev. Biophys.* 33 (2000) 161–197.
- [5] J.C.J. Barna, E.D. Laue, Conventional and exponential sampling for 2D NMR experiments with application to a 2D NMR spectrum of a protein, *J. Magn. Reson.* 75 (1987) 384–389.
- [6] J.C.J. Barna, E.D. Laue, M.R. Mayger, J. Skilling, S.J.P. Worrall, Exponential sampling, an alternative method for sampling in two-dimensional NMR experiments, *J. Magn. Reson.* 73 (1987) 69–77.
- [7] B.E. Coggins, R.A. Venters, P. Zhou, Generalized reconstruction of n-D NMR spectra from multiple projections: application to the 5-D HACACONH spectrum of protein G B1 domain, *J. Am. Chem. Soc.* 126 (2004) 1000–1001.
- [8] B.E. Coggins, R.A. Venters, P. Zhou, Filtered backprojection for the reconstruction of a high-resolution (4, 2)D CH₃–NH NOESY spectrum on a 29 kDa protein, *J. Am. Chem. Soc.* 127 (2005) 11562–11563.
- [9] B.E. Coggins, P. Zhou, Polar Fourier transforms of radially sampled NMR data, *J. Magn. Reson.* 182 (2006) 84–95.
- [10] B.E. Coggins, P. Zhou, Sampling of the NMR time domain along concentric rings, *J. Magn. Reson.* 184 (2007) 219–233.
- [11] K. Ding, A.M. Gronenborn, Novel 2D triple-resonance NMR experiments for sequential resonance assignments of proteins, *J. Magn. Reson.* 156 (2002) 262–268.
- [12] H.R. Eghbalnia, A. Bahrami, M. Tonelli, K. Hallenga, J.L. Markley, High-resolution iterative frequency identification for NMR as a general strategy for multidimensional data collection, *J. Am. Chem. Soc.* 127 (2005) 12528–12536.
- [13] R. Freeman, E. Kupče, New methods for fast multidimensional NMR, *J. Biomol. NMR* 27 (2003) 101–113.
- [14] R. Freeman, E. Kupče, Distant echoes of the accordion: reduced dimensionality, GFT-NMR, and projection-reconstruction of multidimensional spectra, *Concepts Magn. Reson.* 23A (2004) 63–75.
- [15] S. Hiller, F. Fiorito, K. Wüthrich, G. Wider, Automated projection spectroscopy (APSY), *Proc. Natl. Acad. Sci. USA* 102 (2005) 10876–10881.
- [16] K. Kazimierczuk, W. Koźmiński, I. Zhukov, Two-dimensional Fourier transform of arbitrarily sampled NMR data sets, *J. Magn. Reson.* 179 (2006) 323–328.
- [17] K. Kazimierczuk, A. Zawadzka, W. Koźmiński, Optimization of random time domain sampling in multidimensional NMR, *J. Magn. Reson.* 192 (2008) 123–130.
- [18] K. Kazimierczuk, A. Zawadzka, W. Koźmiński, I. Zhukov, Random sampling of evolution time space and Fourier transform processing, *J. Biomol. NMR* 36 (2006) 157–168.
- [19] K. Kazimierczuk, A. Zawadzka, W. Koźmiński, I. Zhukov, Lineshapes and artifacts in multidimensional Fourier transform of arbitrarily sampled NMR data sets, *J. Magn. Reson.* 188 (2007) 344–356.
- [20] S. Kim, T. Szyperki, G.F.T. NMR, A new approach to rapidly obtain precise high-dimensional NMR spectral information, *J. Am. Chem. Soc.* 125 (2003) 1385–1393.
- [21] W. Koźmiński, I. Zhukov, Multiple quadrature detection in reduced dimensionality experiments, *J. Biomol. NMR* 26 (2003) 157–166.
- [22] E. Kupče, R. Freeman, Reconstruction of the three-dimensional NMR spectrum of a protein from a set of plane projections, *J. Biomol. NMR* 27 (2003) 383–387.
- [23] D. Malmodin, M. Billeter, Multiway decomposition of NMR spectra with coupled evolution periods, *J. Am. Chem. Soc.* 127 (2005) 13486–13487.
- [24] D. Marion, Processing of ND NMR spectra sampled in polar coordinates: a simple Fourier transform instead of a reconstruction, *J. Biomol. NMR* 36 (2006) 45–54.
- [25] V.Y. Orekhov, I. Ibragimov, M. Billeter, Optimizing resolution in multidimensional NMR by three-way decomposition, *J. Biomol. NMR* 27 (2003) 165–173.
- [26] N. Pannetier, K. Houben, L. Blanchard, D. Marion, Optimized 3D-NMR sampling for resonance assignment of partially unfolded proteins, *J. Magn. Reson.* 186 (2007) 142–149.
- [27] D. Rovnyak, D.P. Frueh, M. Sastry, Z.Y. Sun, A.S. Stern, J.C. Hoch, G. Wagner, Accelerated acquisition of high resolution triple-resonance spectra using non-uniform sampling and maximum entropy reconstruction, *J. Magn. Reson.* 170 (2004) 15–21.
- [28] P. Schmieder, A.S. Stern, G. Wagner, J.C. Hoch, Improved resolution in triple-resonance spectra by nonlinear sampling in the constant-time domain, *J. Biomol. NMR* 4 (1994) 483–490.
- [29] J.P. Simorre, B. Brutscher, M.S. Caffrey, D. Marion, Assignment of NMR spectra of proteins using triple-resonance two-dimensional experiments, *J. Biomol. NMR* 4 (1994) 325–333.
- [30] T. Szyperki, G. Wider, J.H. Bushweller, K. Wüthrich, 3D 13C–15N-heteronuclear two-spin coherence spectroscopy for polypeptide backbone assignments in 13C–15N-double-labeled proteins, *J. Biomol. NMR* 3 (1993) 127–132.
- [31] T. Szyperki, G. Wider, J.H. Bushweller, K. Wüthrich, Reduced dimensionality in triple-resonance NMR experiments, *J. Am. Chem. Soc.* 115 (1993) 9307–9308.
- [32] R.A. Venters, B.E. Coggins, D. Kojetin, J. Cavanagh, P. Zhou, (4, 2)D Projection-reconstruction experiments for protein backbone assignment: application to human carbonic anhydrase II and calbindin D(28K), *J. Am. Chem. Soc.* 127 (2005) 8785–8795.
- [33] B.E. Coggins, P. Zhou, High resolution 4-D spectroscopy with sparse concentric shell sampling and FFT-CLEAN, *J. Biomol. NMR* (2008).
- [34] G.E. Sarty, The relationship between the Nyquist criterion and the point spread function, *Concepts Magn. Reson.* 17B (2003) 17–24.
- [35] A. Meissner, O.W. Sorensen, Suppression of diagonal peaks in TROSY-type ¹H NMR NOESY spectra of ¹⁵N-labeled proteins, *J. Magn. Reson.* 140 (1999) 499–503.
- [36] G.S. Harbison, J. Feigon, D.J. Ruben, J. Herzfeld, R.G. Griffin, Diagonal peak suppression in 2D-NOE spectra, *J. Am. Chem. Soc.* (1985) 5567–5569.
- [37] J. Wu, J.S. Fan, S.M. Pascal, D. Yang, General method for suppression of diagonal peaks in heteronuclear-edited NOESY spectroscopy, *J. Am. Chem. Soc.* 126 (2004) 15018–15019.
- [38] K.V. Pervushin, G. Wider, R. Riek, K. Wüthrich, The 3D NOESY-[1H,15N,1H]-ZQ-TROSY NMR experiment with diagonal peak suppression, *Proc. Natl. Acad. Sci. USA* 96 (1999) 9607–9612.
- [39] A. Meissner, O.W. Sorensen, Three-dimensional NMR TROSY-type ¹⁵N-resolved ¹H^N–¹H^N NOESY spectra with diagonal peak suppression, *J. Magn. Reson.* 142 (2000) 195–198.
- [40] G. Zhu, Y. Xia, K.H. Sze, X. Yan, 2D and 3D TROSY-enhanced NOESY of ¹⁵N labeled proteins, *J. Biomol. NMR* 14 (1999) 377–381.
- [41] Y. Xia, K. Sze, G. Zhu, Transverse relaxation optimized 3D and 4D ¹⁵N/¹⁵N separated NOESY experiments of ¹⁵N labeled proteins, *J. Biomol. NMR* 18 (2000) 261–268.
- [42] D. Nietispach, Suppression of anti-TROSY lines in a sensitivity enhanced gradient selection TROSY scheme, *J. Biomol. NMR* 31 (2005) 161–166.
- [43] K.V. Pervushin, G. Wider, K. Wüthrich, Single transition-to-single transition polarization transfer (ST2-PT) in [¹⁵N,¹H]-TROSY, *J. Biomol. NMR* 12 (1998) 345–348.